Title

MAJOR OXIDE, MINOR OXIDE, AND TRACE ELEMENT ANALYSIS OF CHERT AND QUARTZITE SOURCE MATERIAL FROM THE HARTVILLE UPLIFT, SOUTHEASTERN WYOMING

Author

Shackley, M. Steven

Publication Date

2017-05-03

GEOARCHAEOLOGICAL XRF LAB
A Green Solar Facility

GEOARCHAEOLOGICAL X-RAY FLUORESCENCE SPECTROMETRY LABORATORY
8100 Wyoming Blvd., Ste M4-158 Albuquerque, NM 87113 USA

MAJOR OXIDE, MINOR OXIDE, AND TRACE ELEMENT ANALYSIS OF CHERT AND QUARTZITE SOURCE MATERIAL FROM THE HARTVILLE UPLIFT, SOUTHEASTERN WYOMING

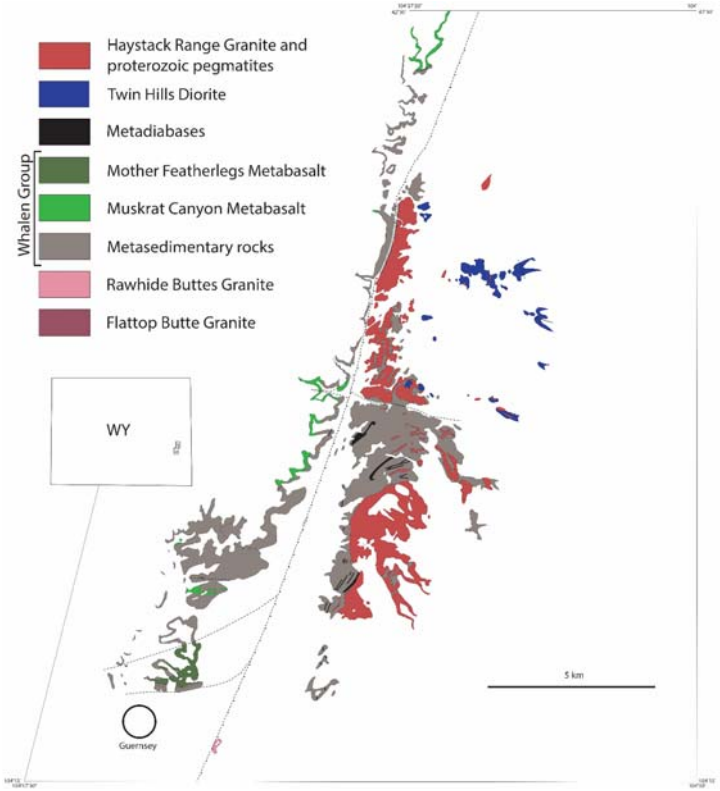

The Hartville Uplift (from Manjón-Cabeza Córdoba 2016)

by

M. Steven Shackley, Ph.D., Director
Geoarchaeological XRF Laboratory
Albuquerque, New Mexico

Report Prepared for

Adam Whitney Guinard
Department of Anthropology
University of Wyoming
Laramie, Wyoming

3 May 2017

INTRODUCTION

The analysis here of chert and quartzite source samples from the Hartville Uplift, Wyoming indicates relatively low variability in the chert samples, and somewhat higher variability in the quartzite samples, particularly in the major and minor oxides and some of the trace elements such as strontium and barium. Also, a previously unpublished analysis by this lab of Spanish Diggings, Wyoming chert for Bruce Huckell at the University of New Mexico is compared to the Hartville chert using the oxides of potassium and calcium, and trace elements Zn and Zr (see also Shackley 1999). This study is mainly seen as an exploratory exercise compositionally documenting the Hartville Uplift chert and quartzite. The comparison with the Spanish Diggings samples is for illustrative purposes.

LABORATORY SAMPLING, ANALYSIS AND INSTRUMENTATION

All samples are analyzed whole. The results presented here are quantitative in that they are derived from "filtered" intensity values ratioed to the appropriate x-ray continuum regions through a least squares fitting formula rather than plotting the proportions of the net intensities in a ternary system (McCarthy and Schamber 1981; Schamber 1977). Or more essentially, these data through the analysis of international rock standards, allow for inter-instrument comparison with a predictable degree of certainty (Hampel 1984; Shackley 2011).

All analyses for this study were conducted on a ThermoScientific *Quant'X* EDXRF spectrometer, located at the Geoarchaeological XRF Laboratory, Albuquerque, New Mexico. It is equipped with a thermoelectrically Peltier cooled solid-state Si(Li) X-ray detector, with a 50 kV, 50 W, ultra-high-flux end window bremsstrahlung, Rh target X-ray tube and a 76 μm (3 mil) beryllium (Be) window (air cooled), that runs on a power supply operating from 4-50 kV/0.02-1.0 mA at 0.02 increments. The spectrometer is equipped with a 200 l min^{-1} Edwards vacuum pump, allowing for the analysis of lower-atomic-weight elements between sodium (Na) and

titanium (Ti). Data acquisition is accomplished with a pulse processor and an analogue-to-digital converter. Elemental composition is identified with digital filter background removal, least squares empirical peak deconvolution, gross peak intensities and net peak intensities above background.

Trace Element Analysis

In the analysis for mid Zb/Zc condition elements Ti-Nb, Pb, Th, the x-ray tube is operated at 30 kV, using a 0.05 mm (medium) Pd primary beam filter in an air path at 100 seconds livetime to generate x-ray intensity Ka-line data for elements titanium (Ti), manganese (Mn), iron (as $Fe_2O_3^T$), cobalt (Co), nickel (Ni), copper, (Cu), zinc, (Zn), gallium (Ga), rubidium (Rb), strontium (Sr), yttrium (Y), zirconium (Zr), niobium (Nb), lead (Pb), and thorium (Th). Not all these elements are reported since their values in many volcanic rocks are very low. Trace element intensities were converted to concentration estimates by employing a linear calibration line ratioed to the Compton scatter established for each element from the analysis of international rock standards certified by the National Institute of Standards and Technology (NIST), the US. Geological Survey (USGS), Canadian Centre for Mineral and Energy Technology, and the Centre de Recherches Pétrographiques et Géochimiques in France (Govindaraju 1994). Line fitting is linear (XML) for all elements. When barium (Ba) is analyzed in the High Zb condition, the Rh tube is operated at 50 kV and up to 1.0 mA, ratioed to the bremsstrahlung region (see Davis 2011; Shackley 2011). Further details concerning the petrological choice of these elements in Southwest volcanic rocks is available in Shackley (1988, 1995, 2005; also Mahood and Stimac 1991; and Hughes and Smith 1993). Nineteen specific pressed powder standards are used for the best fit regression calibration for elements Ti-Nb, Pb, Th, and Ba, and include G-2 (basalt), AGV-2 (andesite), GSP-2 (granodiorite), SY-2 (syenite), BHVO-2 (hawaiite), STM-1 (syenite), QLO-1 (quartz latite), RGM-1 (obsidian), W-2 (diabase),

BIR-1 (basalt), SDC-1 (mica schist), TLM-1 (tonalite), SCO-1 (shale), NOD-A-1 and NOD-P-1 (manganese) all US Geological Survey standards, NIST-278 (obsidian), U.S. National Institute of Standards and Technology, BE-N (basalt) from the Centre de Recherches Pétrographiques et Géochimiques in France, and JR-1 and JR-2 (obsidian) from the Geological Survey of Japan (Govindaraju 1994).

Major and Minor Oxide Analysis

Analysis of the major oxides of Si, Al, Ca, Fe, K, Mg, Mn, Na, and Ti is performed under the multiple conditions elucidated below. This fundamental parameter analysis (theoretical with standards), while not as accurate as destructive analyses (pressed powder and fusion disks) is usually within a few percent of actual, based on the analysis of USGS RGM-1 obsidian standard (see also Shackley 2011). The fundamental parameters (theoretical) method is run under conditions commensurate with the elements of interest and calibrated with 11 USGS standards (RGM-1, rhyolite; AGV-2, andesite; BHVO-1, hawaiite; BIR-1, basalt; G-2, granite; GSP-2, granodiorite; BCR-2, basalt; W-2, diabase; QLO-1, quartz latite; STM-1, syenite), and one Japanese Geological Survey rhyolite standard (JR-1). See Lundblad et al. (2011) for another set of conditions and methods for oxide analyses.

Conditions Of Fundamental Parameter Analysis[1]:

Low Za (Na, Mg, Al, Si, P)

Voltage	6 kV	Current	Auto[2]
Livetime	100 seconds	Counts Limit	0
Filter	No Filter	Atmosphere	Vacuum
Maximum Energy	10 keV	Count Rate	Low

Low Zb (S, Cl, K, Ca)

Voltage	8 kV	Current	Auto
Livetime	100 seconds	Counts Limit	0
Filter	Cellulose (0.06 mm)	Atmosphere	Vacuum
Maximum Energy	10 keV	Count Rate	Low

Mid Zb (K, Ca, Ti, V, Cr, Mn, Fe)

Voltage	32 kV	Current	Auto
Livetime	100 seconds	Counts Limit	0
Filter	Pd (0.06 mm)	Atmosphere	Vacuum
Maximum Energy	40 keV	Count Rate	Medium

High Zb (Sn, Sb, Ba, Ag, Cd)

Voltage	50 kV	Current	Auto
Livetime	100 seconds	Counts Limit	0
Filter	Cu (0.559 mm)	Atmosphere	Vacuum
Maximum Energy	40 keV	Count Rate	High

[1] Multiple conditions designed to ameliorate peak overlap identified with digital filter background removal, least squares empirical peak deconvolution, gross peak intensities and net peak intensities above background.

[2] Current is set automatically based on the mass absorption coefficient.

Statistical and Graphical Source Assignment.

The data from the WinTrace^{TM} software were translated directly into Excel for Windows software for manipulation and on into SPSS, ver. 21 for Windows for statistical analyses. In order to evaluate these quantitative determinations, machine data were compared to measurements of known standards during each run. RGM-1 a USGS rhyolite obsidian standard is analyzed during each sample run of ≤ 20 samples for the samples to insure machine calibration (Tables 1 and 2).

The elemental concentrations were investigated by a stepped statistical and graphical method, outlined in Shackley et al. (2017). In secondary siliceous sediments and metamorphic rocks the proportion of SiO_2 comprises over 88%, and often over 98% of the composition, so the remainder of the oxides and trace elements is very small and rarely exhibiting much variability, particularly since XRF does not have the instrumental precision often required for the analysis of these rocks (see Church 1990; Gauthier et al. 2012; Huckell et al. 2011; Luedtke 1992; Luedtke and Myers 1984; Malyk-Selivanova et al. 1998; Nazaroff 2016; Warashina 1992; Figures 2 through 5 here).

Having said that, there is variability that can be discerned in some cases, and discussed by Gauthier et al. (2012) in their study of northeastern North American chert using XRF as in this study here of the Hartville Uplift chert and a sample of Spanish Diggings, Wyoming chert collected by Bruce Huckell and analyzed by this lab in 2012. Often potassium (K) and calcium (Ca) oxides are useful in discriminating cherts, at least in some cases (Gauthier et al. 2012). A bivariate plot of these two oxides using the Hartville and Spanish Diggings data indicates that uniformly Spanish Diggings exhibits a much lower proportion of these oxides (see Figures 2 and 3). However, they do overlap to a small degree, but there are only five samples available from the Spanish Diggings source, so there could be greater variability that evident in this sample, as evident in the cluster dendrogram (Figure 3). Perhaps more useful, the elements Zn and Zr proved to be helpful in discriminating Spanish Diggings from the Hartville rocks, although the small sample caveat still stands (Figures 2 and 3).

The Hartville Uplift Rocks

The analysis here of the Hartville Uplift chert and quartzite is one of the first using XRF on these rocks (see Shackley 1999). The Hartville Uplift is a structural arch that connects the Laramie Range with the southern Black Hills. It is about 25 miles (north to south) by about 45

miles (east to west; see Figure 1 here). The Laramie Range is to the west and the North Platte River flows along the uplift's western and southern boundaries (Manjón-Cabeza Córdoba 2016). Laramide-age uplift exposes a complex setting of Archean and Paleoproterozoic rocks that crop out at various points; this includes the chert and quartzites here that are part of the Whalen Group (Manjón-Cabeza Córdoba 2016; Simms and Day 1999; Figure 1 here). These are very old rocks, in part the reason there is so much variability in the quartzite. Interestingly, the chert, which as a secondary sediment is not quite as old and does not exhibit the level of variability suggests that metamorphic processes are not acute.

DISCUSSION OF RESULTS

The data were examined for those element and oxides that appear to exhibit the greatest variability (c.f. Gauthier et al. 2012; Nazaroff 2016; see Tables 2 through 4 here). Immediately apparent, besides the alkalis and salts typically used to discriminate secondary siliceous sediment and metamorphic rocks (i.e. K and Ca) is the variability in Sr and Ba for both rock types (Figures 4 and 5). It is not clear why these transition metals are variable in the rocks, likely a pattern in Hartville Uplift sediments, but serves as a viable analytical strategy.

While the use of XRF in the analysis of metamorphic and secondary siliceous rocks can be hazardous, there are some results that show potential here. Some of the major oxides and trace elements seem distinctive, and the comparison with Spanish Diggings chert seems promising as well. Again the Spanish Diggings sample is small, so the variability seen here could be greater with an enlarged sample.

REFERENCES CITED

Church, T. 1990, *An investigation into prehistoric lithic procurement in the Bearlodge Mountains, Wyoming*. Masters thesis, Department of Anthropology, University of Montana, Missoula.

Davis, M.K., T.L. Jackson, M.S. Shackley, T. Teague, and J. Hampel, 2011, Factors Affecting the Energy-Dispersive X-Ray Fluorescence (EDXRF) Analysis of Archaeological Obsidian. In *X-Ray Fluorescence Spectrometry (XRF) in Geoarchaeology*, edited by M.S. Shackley, pp. 45-64. Springer, New York.

Govindaraju, K., 1994, 1994 Compilation of Working Values and Sample Description for 383 Geostandards. *Geostandards Newsletter* 18 (special issue).

Gauthier G., A.L. Burke, and M. Leclerc, 2012, Assessing XRF for the geochemical characterization of radiolarian chert artifacts from northeastern North America. *Journal of Archaeological Science* 39:2436-2451.

Hampel, Joachim H., 1984, Technical Considerations in X-ray Fluorescence Analysis of Obsidian. In *Obsidian Studies in the Great Basin*, edited by R.E. Hughes, pp. 21-25. Contributions of the University of California Archaeological Research Facility 45. Berkeley.

Hildreth, W., 1981, Gradients in Silicic Magma Chambers: Implications for Lithospheric Magmatism. *Journal of Geophysical Research* 86:10153-10192.

Huckell, B.B., J.D. Kilby, M.T. Boulanger, and M.D. Glascock, 2011, Sentinel Butte: neutron activation analysis of White River Group chert from a primary source and artifacts from a Clovis cache in North Dakota, USA. *Journal of Archaeological Science* 38:965-976.

Hughes, Richard E., and Robert L. Smith, 1993, Archaeology, Geology, and Geochemistry in Obsidian Provenance Studies. *In Scale on Archaeological and Geoscientific Perspectives*, edited by J.K. Stein and A.R. Linse, pp. 79-91. Geological Society of America Special Paper 283.

Luedtke, B.E. 1992, *An Archaeologists Guide to Chert and Flint*. Archaeological Research Tools 7, Institute of Archaeology, University of California, Los Angeles.

Luedtke, B.E. and J.T. Meyers, 1984, Trace element variation in Burlington chert: a case study. In Butler, B.M., and May E.E. (Eds.), pp. 287-298. *Prehistoric Chert Exploration: Studies from the Mid-Continent*. Center for Archaeological Investigations Occasional Paper 2. Carbondale: Southern Illinois University.

Lundblad, S.P., P.R. Mills, A. Drake-Raue, and S.K. Kikiloi, 2011, Non-destructive EDXRF analyses of archaeological basalts. In *In M.S. Shackley (Ed.) X-Ray Fluorescence Spectrometry (XRF) in Geoarchaeology*, pp. 65-80. Springer Publishing, New York.

Mahood, Gail A., and James A. Stimac, 1990, Trace-Element Partitioning in Pantellerites and Trachytes. *Geochemica et Cosmochimica Acta* 54:2257-2276.

Malyk-Selivanova, N., G.M. Ashley, R. Gal, M.D. Glascock, and H. Neff, 1998, Geological-geochemical approach to "sourcing" of prehistoric chert artifacts, northwestern Alaska. *Geoarchaeology* 13:673-708.

Manjón-Cabeza Córdoba, 2016, *Geochemistry, petrogenesis and tectonic setting of igneous rocks of the Hartville Uplift, eastern Wyoming*. Masters thesis, Department of Geological Sciences, University of Missouri, Columbia.

McCarthy, J.J., and F.H. Schamber, 1981, Least-Squares Fit with Digital Filter: A Status Report. In *Energy Dispersive X-ray Spectrometry*, edited by K.F.J. Heinrich, D.E. Newbury, R.L. Myklebust, and C.E. Fiori, pp. 273-296. National Bureau of Standards Special Publication 604, Washington, D.C.

Nazaroff, A., 2016, *Entanglement: A Study in Neolithic Resource Exploitation in the Middle East,* Ph.D. dissertation, Department of Anthropology, Stanford University.

Schamber, F.H., 1977, A Modification of the Linear Least-Squares Fitting Method which Provides Continuum Suppression. In *X-ray Fluorescence Analysis of Environmental Samples*, edited by T.G. Dzubay, pp. 241-257. Ann Arbor Science Publishers.

Shackley, M.S., 1988, Sources of archaeological obsidian in the southwest: an archaeological, petrological, and geochemical study. *American Antiquity* 53:752-772.

Shackley, M. S.,1995, Sources of archaeological obsidian in the greater american southwest: an update and quantitative analysis. *American Antiquity* 60(3):531-551.

Shackley, M.S., 1999, An energy-dispersive x-ray fluorescence (EDXRF) analysis of metamorphic and secondary siliceous sediment source and archaeological stone from northeastern Wyoming. Report prepared for TRC Mariah Associates, Inc., Laramie, Wyoming.

Shackley, M.S., 2005, *Obsidian: Geology and Archaeology in the North American Southwest*. University of Arizona Press, Tucson.

Shackley, M.S., 2011, An Introduction to X-Ray Fluorescence (XRF) Analysis in Archaeology. In *X-Ray Fluorescence Spectrometry (XRF) in Geoarchaeology*, M.S. Shackley (Ed.), pp. 7-44. Springer, New York.

Shackley, M.S., L.E. Morgan, and D. Pyle, 2017, Elemental, isotopic, and geochronological variability in Mogollon-Datil Volcanic Province archaeological obsidian, southwestern New Mexico: solving issues of inter-source discrimination. *Geoarchaeology,* in press.

Sims, P. K., and Day, W. C., compilers, 1999, Geologic map of Precambrian rocks of the Hartville Uplift, southeastern Wyoming with a section on mineral deposits in the Hartville Uplift by Terry Klein. U. S. Geological Survey MAP I-2661, scale 1:48,000, 1 sheet, 30 p. text.

Warashina, T., 1992, Allocations of jasper archaeological implements by means of ESR and XRF. *Journal of Archaeological Science* 19:357-373.

Table 1. Major and minor oxide concentrations for the USGS RGM-1 standard used during this analysis. All measurements in percent by weight.

Sample (%)	SiO_2	Al_2O_3	CaO	Fe_2O_3T	K_2O	MgO	MnO	Na_2O	TiO_2	Σ
RGM-1 (USGS recommended)	73.4±0.53	13.7±0.19	1.15±0.07	1.86±0.01	4.30±0.10	0.28±0.03	0.036±0.004	4.07±0.15	0.27±0.02	99.06
RGM-1 (this study, N=4))	73.9±0.1	13.1±0.1	1.40±0.0	2.20±0.0	4.9±0.0	<0.1±	0.0±	3.90±0.1	0.30±0.0	99.70

Table 2. Trace element concentrations for the USGS RGM-1 rhyolite standard used during this analysis. All measurements in parts per million (ppm).

SAMPLE (ppm)	Cu	Zn	Ga	Rb	Sr	Y	Zr	Nb	Ba
RGM-1 (USGS recommended)	10.2±1.7	32±n.r.	15±2	150±8	110±10	25±n.r.	220±20	8.9±0.6	810±46
RGM-1, pressed powder (this study, n=4)	12±1.4	39.7±1.5	16.8±0.9	147±4	108±4	27±1	220±2	10±2.3	866±59

n.r.=no report

Table 3. Major, minor oxides and trace element concentrations for the Hartville Uplift chert source specimens.

Sample	Locality	Na2O	MgO	Al2O3	SiO2	K2O	CaO	TiO2	MnO	Fe2O3
		%	%	%	%	%	%	%	%	%
L3-N2	48PL363	2.279	0.133	0	96.357	0.113	0.187	0.009	0.038	0.266
L3-N8	48PL363	1.625	0	0.015	97.174	0.18	0.374	0	0.013	0.298
L3-N19	48PL363	1.416	1.027	0.055	96.919	0.126	0.055	0.032	0.127	0.079
L3-N32	48PL363	1.495	0.03	0.041	97.689	0.134	0.094	0.018	0.091	0.139
L4-N34	48PL363	1.25	0.054	0.333	96.435	0.207	1.379	0.051	0.028	0.109
L3-N41	48PL363	2.092	0.079	0	97.002	0.07	0.062	0.012	0.013	0.151
L3-N48	48PL363	2.263	0	0	96.705	0.107	0.108	0.011	0.052	0.096
FS47	48PL1312	1.425	0.159	0	97.314	0.108	0.293	0.008	0.003	0.608
FS48	48PL1312	1.343	0.121	0.272	95.986	0.242	0.957	0.038	0.077	0.703
FS49	48PL1312	1.846	0.231	0.249	95.35	0.195	1.077	0.027	0.058	0.508
FS50	48PL1312	1.369	0.202	0.252	96.934	0.17	0.304	0.011	0.081	0.53
FS51	48PL1312	1.175	0.044	0.033	98.215	0.124	0.141	0.003	0.012	0.207
FS52	48PL1312	1.306	0.191	0.052	97.932	0.156	0.103	0.009	0.008	0.169
FS53	48PL1312	1.287	0.453	1.263	96.195	0.273	0.14	0.005	0.023	0.24
FS54	48PL2034	1.372	0.274	0	97.161	0.073	0.721	0.01	0.015	0.124
FS55	48PL2034	1.16	0.224	0	98.311	0.078	0.049	0.009	0.003	0.116
FS56	48PL2034	1.474	1.798	0	96.072	0.111	0.122	0.016	0.005	0.171
FS57	48PL2034	1.166	0.173	0.029	98.109	0.105	0.187	0.021	0	0.126
FS58	48PL2034	1.314	0.475	0	97.715	0.097	0.093	0.015	0.029	0.141
FS59	48PL2034	1.269	0.912	0.07	96.977	0.119	0.3	0.002	0.056	0.133
FS60	48PL2034	1.091	0.212	0	98.243	0.076	0.133	0.009	0.026	0.116
FS40	48PL2215	1.157	0.283	0.802	96.975	0.196	0.156	0.03	0.004	0.232
FS41	48PL2215	0.957	0.126	0.139	98.287	0.15	0.125	0.033	0.017	0.109
FS42	48PL2215	1.194	0.189	0.096	97.94	0.132	0.11	0.03	0.048	0.189
FS43	48PL2215	1.411	0.056	0.058	97.788	0.128	0.095	0.011	0.095	0.224
FS44	48PL2215	1.349	0.264	0.456	96.83	0.253	0.189	0.022	0.007	0.508
FS45	48PL2215	1.212	0.227	0.066	97.898	0.131	0.109	0.016	0.012	0.227
FS46	48PL2215	1.003	0.364	0.154	97.908	0.195	0.104	0.012	0.069	0.111
1-FS2	48PL2206	1.363	0.345	1.31	96.243	0.214	0.094	0.003	0.001	0.315
3-FS3	48PL2207	1.211	0.58	1.208	95.843	0.359	0.086	0.025	0.011	0.594
4-FS4	48PL2208	1.241	0.333	0.811	96.766	0.209	0.086	0.032	0.011	0.318

Sample	Locality	Na2O	MgO	Al2O3	SiO2	K2O	CaO	TiO2	MnO	Fe2O3
1-FS1	48PL2213	1.36	0.255	0.418	97.192	0.166	0.1	0.021	0.012	0.318
22-FS7	48PL2231	1.368	0.625	1.016	95.715	0.316	0.337	0.017	0.011	0.417
		Cu	**Zn**	**Ga**	**Rb**	**Sr**	**Y**	**Zr**	**Nb**	**Ba**
		ppm	ppm	ppm	ppm	ppm	ppm	ppm	ppm	ppm
LN-N2	48PL363	8	16	11	0	19	8	18	1	162
LN-N8	48PL363	5	22	9	0	19	7	19	2	30
LN-N19	48PL363	3	13	10	2	14	7	23	1	283
LN-N32	48PL363	8	11	8	1	11	5	22	1	280
LN-N34	48PL363	5	13	8	4	28	13	82	1	155
LN-N41	48PL363	3	16	8	0	13	4	17	7	1
LN-N48	48PL363	4	13	8	0	16	6	21	4	178
FS47	48PL1312	16	36	9	0	15	5	16	2	11
FS48	48PL1312	8	20	10	0	41	9	22	1	364
FS49	48PL1312	11	22	8	3	17	5	17	2	254
FS50	48PL1312	5	14	10	0	23	8	23	1	414
FS51	48PL1312	6	19	8	0	15	5	20	1	61
FS53	48PL1312	8	20	10	1	22	5	20	1	62
FS52	48PL1312	7	13	9	2	15	6	21	1	155
FS54	48PL2034	8	14	9	0	10	4	17	1	51
FS55	48PL2034	4	13	9	0	12	4	22	1	9
FS56	48PL2034	4	19	9	0	11	5	23	1	10
FS57	48PL2034	6	17	9	0	14	4	22	1	7
FS58	48PL2034	3	15	8	0	12	6	19	1	117
FS59	48PL2034	4	14	9	0	14	7	20	1	147
FS60	48PL2034	4	15	9	0	12	5	22	2	68
FS40	48PL2215	3	13	8	0	15	10	16	2	1
FS41	48PL2215	1	16	10	0	13	4	24	1	50
FS42	48PL2215	10	16	10	0	19	6	23	1	134
FS43	48PL2215	9	19	12	0	19	4	18	1	322
FS44	48PL2215	1	15	9	0	18	9	27	1	36
FS45	48PL2215	6	14	9	0	17	7	19	1	12
FS46	48PL2215	9	19	9	3	20	9	20	1	148
1-FS2	48PL2206	8	12	9	0	13	7	18	1	17

Sample	Locality	Cu	Zn	Ga	Rb	Sr	Y	Zr	Nb	Ba
3-FS3	48PL2207	4	20	10	7	16	6	28	1	82
4-FS4	48PL2208	10	13	8	0	17	4	18	1	107
1-FS1	48PL2213	2	26	10	0	14	8	19	1	104
22-FS7	48PL2231	2	52	8	6	18	10	24	1	189

Table 4. Major, minor oxides and trace element concentrations for the Hartville Uplift quartzite source specimens.

Sample	Locality	Na2O	MgO	Al2O3	SiO2	K2O	CaO	TiO2	MnO	Fe2O3
FS1	Quarry 1	1.335	0.73	0.26	94.165	0.361	2.876	0.018	0	0.054
FS3	Quarry 1	1.588	0.214	0.455	92.395	0.499	4.627	0.018	0.004	0.082
FS4	Quarry 1	1.419	0.394	0.199	96.729	0.323	0.613	0.044	0.002	0.127
FS5	Quarry 1	1.222	0	0.082	98.072	0.304	0.064	0.021	0.003	0.051
FS7	Quarry 1	1.522	1.227	0.12	95.005	0.25	1.57	0.022	0.002	0.068
FS8	Quarry 1	1.515	2.153	0.265	92.067	0.314	3.338	0.023	0.004	0.074
FS76	Quarry 1	1.572	0.174	0.111	97.576	0.201	0.078	0.026	0.004	0.068
FS10	Quarry 2	1.568	0.152	0.257	97.026	0.307	0.09	0.039	0.001	0.149
FS11	Quarry 2	1.6	0.039	0.24	97.25	0.337	0.08	0.019	0.002	0.116
FS12	Quarry 2	1.584	0.106	0.322	97.207	0.353	0.092	0.024	0	0.089
FS15	Quarry 2	1.411	0.114	0.214	97.612	0.266	0.065	0.014	0.001	0.06
FS16	Quarry 2	1.425	0.122	0.265	97.291	0.394	0.103	0.025	0	0.131
FS17	Quarry 2	1.571	0.087	0.44	97.103	0.409	0.092	0.015	0	0.111
FS18	Quarry 2	1.166	0.125	0.512	95.815	0.425	1.661	0.028	0.005	0.156
FS19	Quarry 3	1.514	0.175	0.408	97.042	0.332	0.067	0.022	0.022	0.073
FS23	Quarry 3	1.361	0.127	0.108	97.622	0.236	0.076	0.039	0.018	0.101
FS24	Quarry 3	1.724	0	0.207	97.085	0.213	0.039	0.007	0.002	0.469
FS25	Quarry 3	1.815	0.033	0.373	96.758	0.321	0.066	0.037	0.025	0.119
FS26	Quarry 3	1.402	0.024	0.443	96.824	0.367	0.148	0.006	0.022	0.534
FS27	Quarry 3	1.86	0.071	0.288	96.822	0.322	0.061	0.021	0.004	0.067
FS29	Quarry 3	1.168	0.013	0.139	97.881	0.236	0.077	0.017	0.017	0.305
FS31	Quarry 4	1.219	0.066	0.141	97.958	0.237	0.074	0.02	0	0.133
FS32	Quarry 4	1.358	0.084	0.226	96.845	0.286	0.198	0.036	0.044	0.637
FS33A	Quarry 4	1.644	0	0.291	97.36	0.255	0.042	0.012	0.002	0.091
FS33B	Quarry 4	1.517	0.129	0.19	97.452	0.243	0.069	0.011	0.024	0.083

Sample	Locality	Na2O	MgO	Al2O3	SiO2	K2O	CaO	TiO2	MnO	Fe2O3
FS34	Quarry 4	1.563	0.086	0.193	97.417	0.258	0.079	0.001	0.003	0.104
FS35	Quarry 4	1.538	0.094	0.297	97.286	0.271	0.117	0.029	0.022	0.077
FS36	Quarry 4	1.661	0.013	0	97.631	0.232	0.049	0	0.009	0.126
1-FS1	48PL2213	1.514	0.317	0.992	96.09	0.323	0.294	0.017	0.012	0.164
1-FS1-14	48PL2214	1.576	0.794	2.309	94.278	0.384	0.204	0.045	0.005	0.257
4-FS4	48PL2226	1.121	0.492	1.158	96.359	0.484	0.069	0.052	0.011	0.184
FS12	48PL2231	2.797	1.576	2.96	88.684	1.121	1.715	0.045	0.05	0.49
FS7	48PL2231	1.51	0.447	0.939	96.386	0.309	0.082	0.019	0.003	0.137
Sample	**Locality**	**Cu**	**Zn**	**Ga**	**Rb**	**Sr**	**Y**	**Zr**	**Nb**	**Ba**
FS1	Quarry 1	7	16	9	8	18	7	51	1	12
FS3	Quarry 1	7	10	9	12	22	4	42	1	48
FS4	Quarry 1	8	17	9	5	17	4	55	2	43
FS5	Quarry 1	3	11	8	6	20	9	38	4	28
FS7	Quarry 1	7	12	10	5	15	4	51	2	23
FS8	Quarry 1	8	11	8	4	18	5	90	4	40
FS76	Quarry 1	6	17	9	1	16	4	41	1	70
FS10	Quarry 2	6	16	9	3	16	8	102	1	58
FS11	Quarry 2	4	12	10	4	20	4	46	1	40
FS12	Quarry 2	3	13	8	5	15	4	56	1	24
FS15	Quarry 2	3	10	9	3	15	10	41	1	16
FS16	Quarry 2	6	13	8	10	18	4	73	5	51
FS17	Quarry 2	3	14	8	3	19	7	61	4	47
FS18	Quarry 2	5	13	9	8	16	5	57	1	32
FS19	Quarry 3	7	13	8	8	21	5	81	1	278
FS23	Quarry 3	2	10	9	1	16	6	29	1	102
FS24	Quarry 3	4	16	8	4	20	4	36	1	142
FS25	Quarry 3	6	15	9	7	21	4	32	1	285
FS26	Quarry 3	8	16	9	6	19	4	50	1	484
FS27	Quarry 3	6	13	8	7	18	6	28	1	107
FS29	Quarry 3	5	15	9	5	17	5	36	1	139
FS31	Quarry 4	3	13	9	0	13	4	27	4	1
FS32	Quarry 4	9	20	10	7	23	7	46	4	724

Sample	Locality	Cu	Zn	Ga	Rb	Sr	Y	Zr	Nb	Ba
FS33A	Quarry 4	8	11	9	6	14	4	30	1	59
FS33B	Quarry 4	7	13	10	2	16	6	37	3	88
FS34	Quarry 4	9	10	8	3	16	7	30	5	0
FS35	Quarry 4	2	14	8	7	15	6	32	1	69
FS36	Quarry 4	3	11	8	3	16	12	62	1	13
1-FS1	48PL2213	8	15	9	4	18	5	48	3	63
1-FS1-14	48PL2214	4	13	9	1	17	6	37	4	44
4-FS4	48PL2226	7	11	9	9	19	4	69	1	175
FS12	48PL2231	3	27	9	4	16	6	31	1	60
FS7	48PL2231	7	15	8	0	20	6	56	5	80

Table 2. Mean and central tendency oxide and elemental concentrations for the chert (left) and quartzite (right). Na-Fe in wt. percent, and Cu-Ba in parts per million (ppm).

	N	Minimum	Maximum	Mean	Std. Deviation
Na2O	33	.957	2.279	1.4	.3
MgO	33	.000	1.798	.3	.4
Al2O3	33	.000	1.310	.3	.4
SiO2	33	95.350	98.311	97.1	.8
K2O	33	.070	.359	.2	.1
CaO	33	.049	1.379	.3	.3
TiO2	33	.000	.051	.0	.0
MnO	33	.000	.127	.0	.0
Fe2O3	33	.079	.703	.3	.2
Cu	33	.5	15.6	5.8	3.3
Zn	33	10.6	51.7	17.9	7.8
Ga	33	8.0	11.6	9.1	.9
Rb	33	.1	6.5	1.5	1.4
Sr	33	10.5	41.2	16.8	5.9
Y	33	3.7	13.1	6.4	2.2
Zr	33	16.5	81.5	22.5	11.0
Nb	33	1.0	6.7	1.4	1.1
Ba	33	1.0	414.2	121.8	112.8

	N	Minimum	Maximum	Mean	Std. Deviation
Na2O	33	1.121	2.797	1.5	.3
MgO	33	.000	2.153	.3	.5
Al2O3	33	.000	2.960	.5	.6
SiO2	33	88.684	98.072	96.3	2.0
K2O	33	.201	1.121	.3	.2
CaO	33	.039	4.627	.6	1.1
TiO2	33	.000	.052	.0	.0
MnO	33	.000	.050	.0	.0
Fe2O3	33	.051	.637	.2	.2
Cu	33	1.5	9.5	5.5	2.2
Zn	33	10.1	27.5	13.8	3.4
Ga	33	8.0	10.3	8.8	.6
Rb	33	.6	12.1	5.0	2.8
Sr	33	13.2	23.2	17.5	2.4
Y	33	3.7	12.0	5.6	2.0
Zr	33	27.3	101.5	48.6	18.4
Nb	33	1.0	5.0	2.1	1.4
Ba	33	1.0	723.7	104.5	148.4

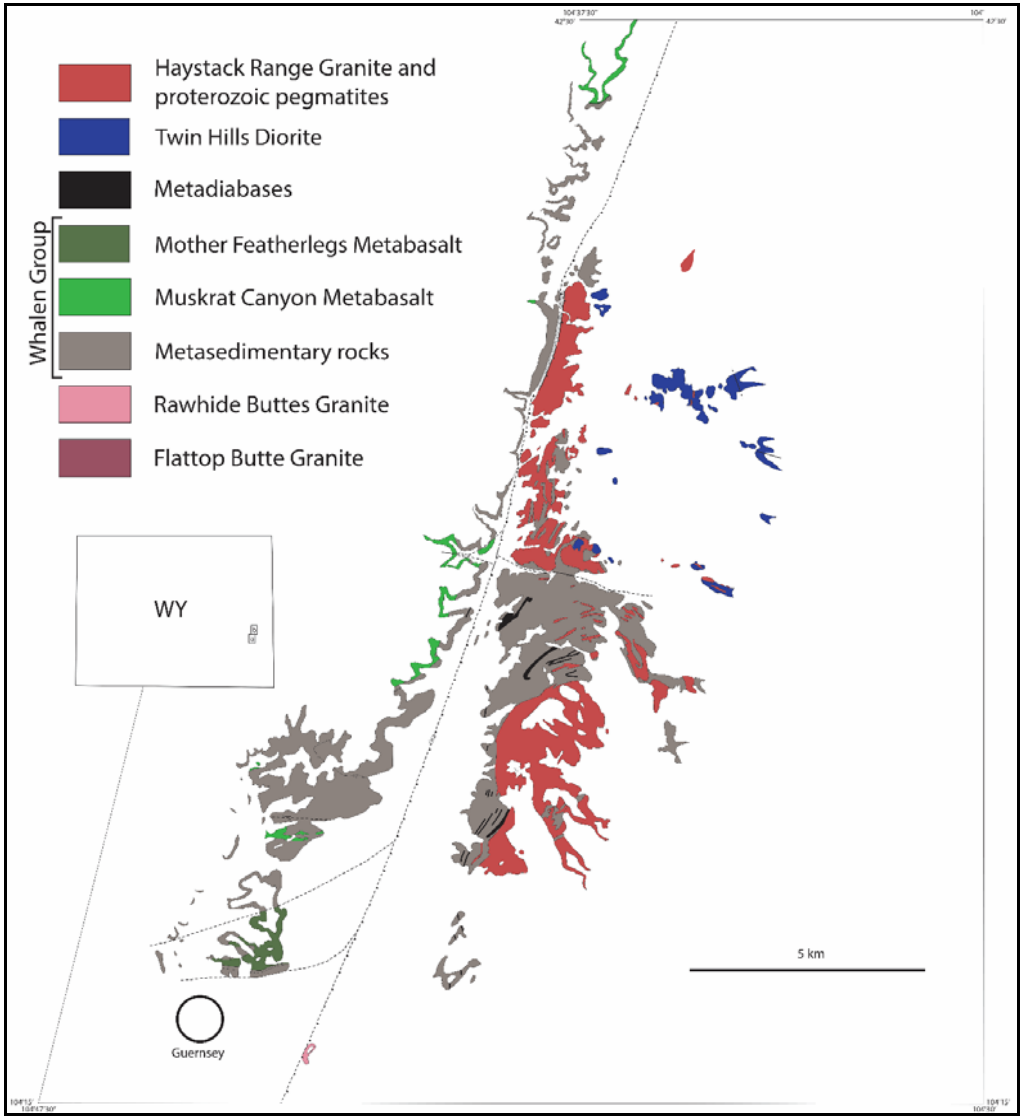

Figure 1. Geologic map of the Hartville Uplift (from Manjón-Cabeza Córdoba 2016:4).

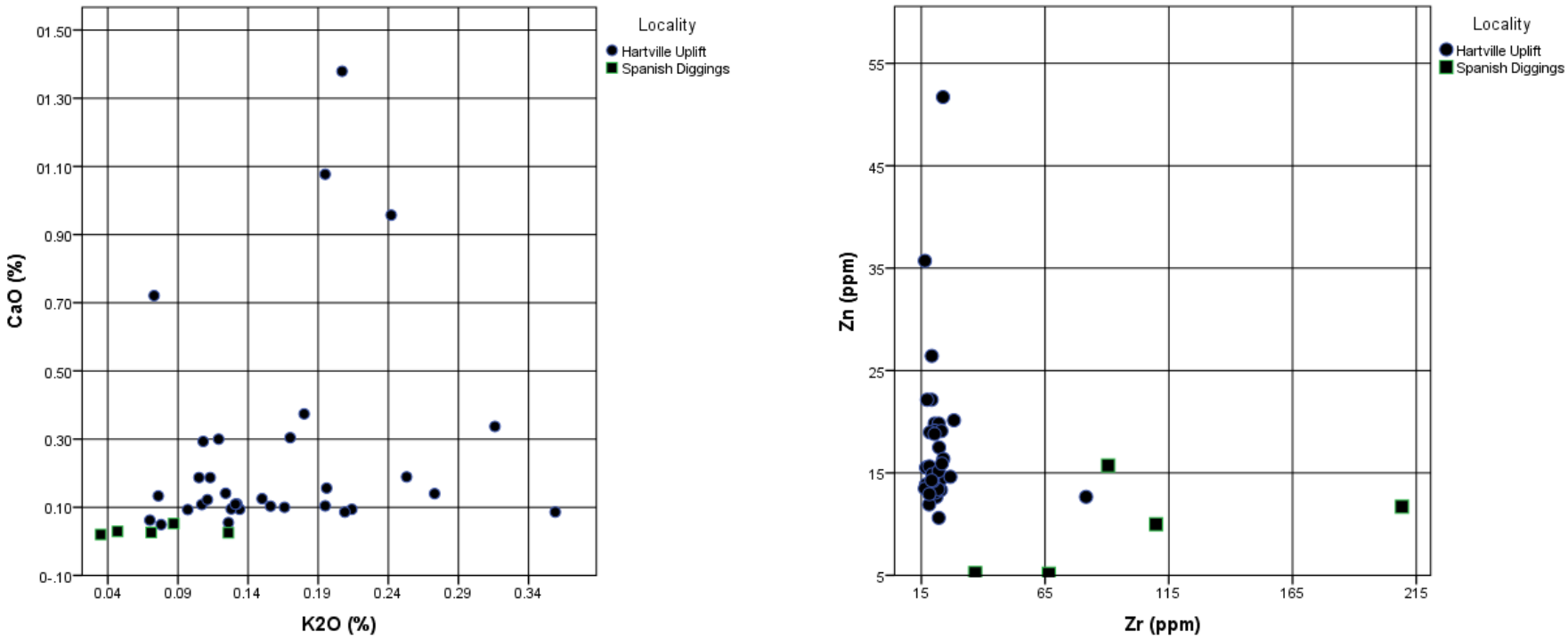

Figure 2. K versus Ca bivariate plot (left) and Zr versus Zn (right) of the Hartville Uplift and Spanish Diggings chert.

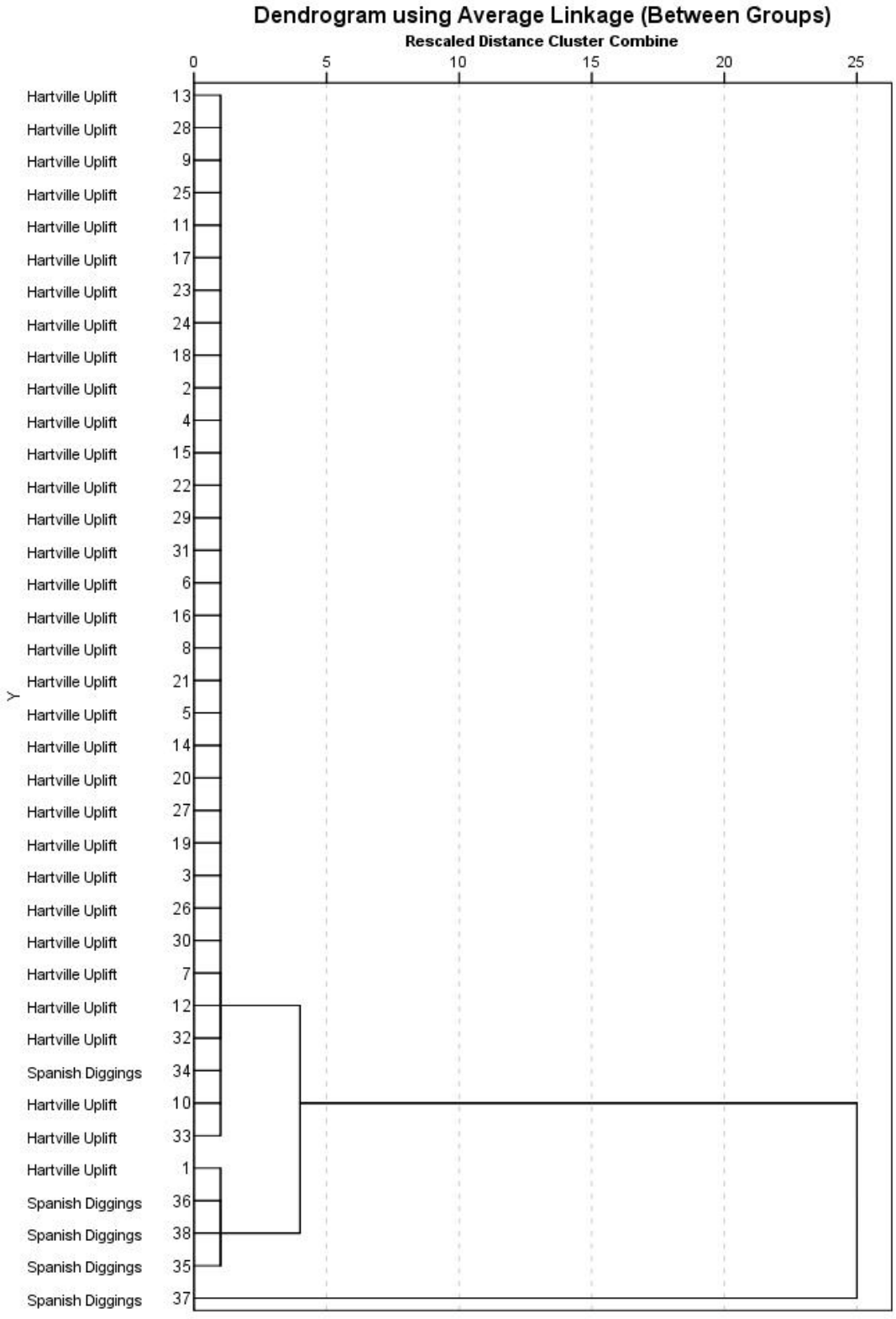

Figure 3. Cluster dendrogram of average linking, squared Euclidean distance using K, Ca, Zn, Zr elements in the analysis (see also Figure 2).

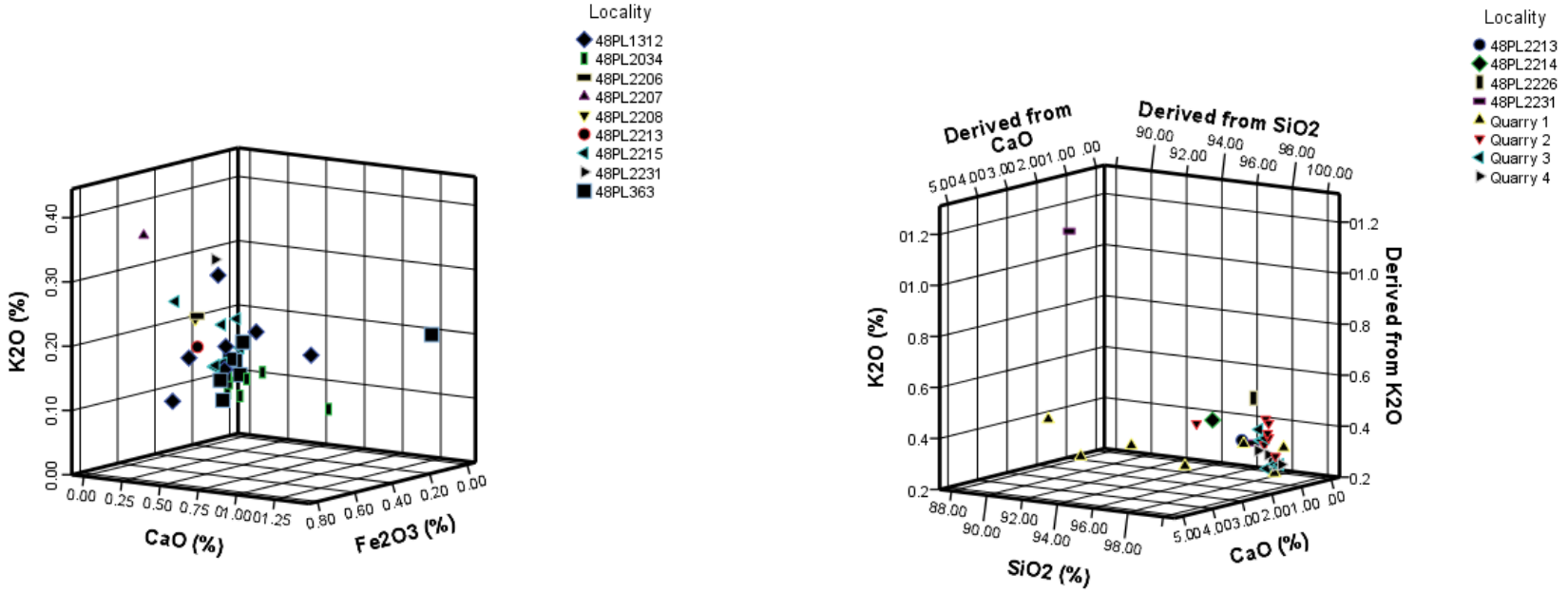

Figure 4. Ca, K, Fe three dimensional plot of the chert specimens (left), and Si, K, Ca plot of the quartzite specimens (right).

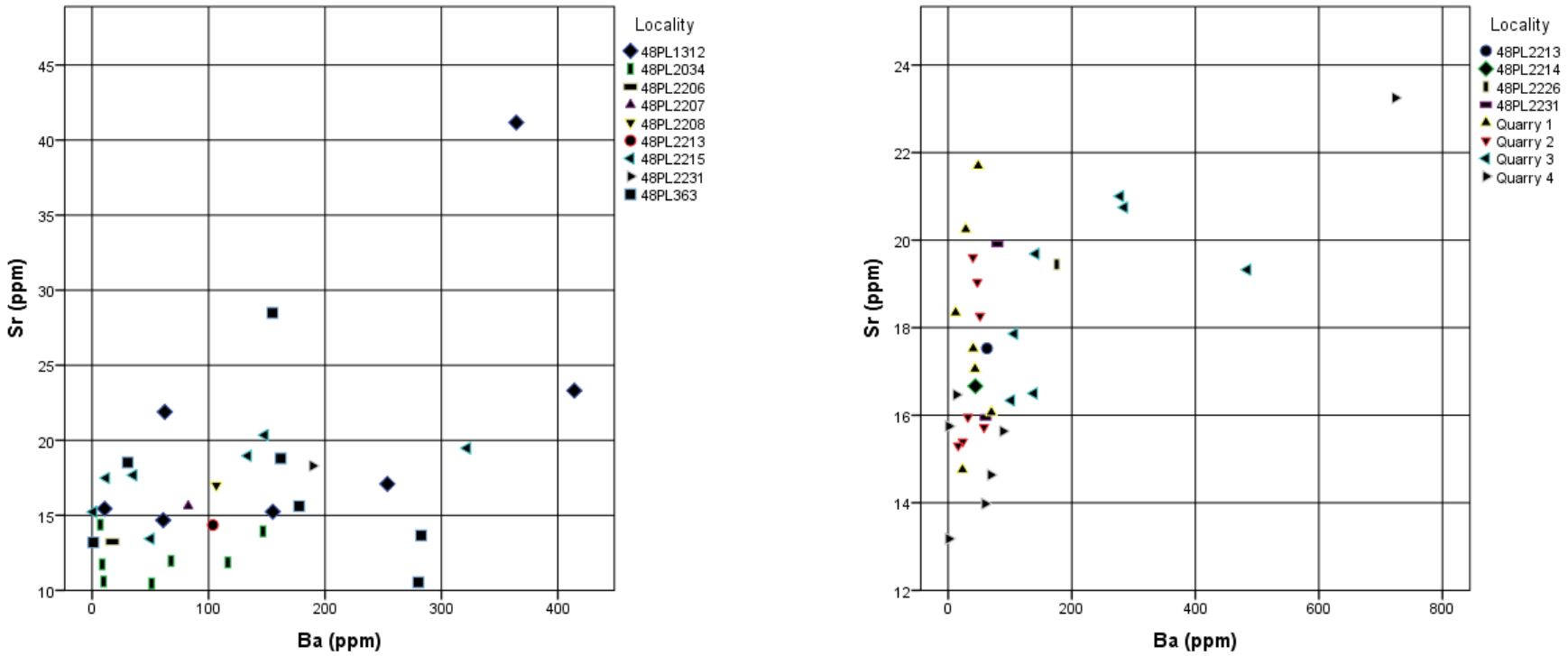

Figure 5. Ba versus Sr bivariate plots of the chert specimens (left) and quartzite specimens (right).